01 Jan 2007

Incorporating the Effects of Magnetic Saturation in a Coupled-Circuit Model of a Claw-Pole Alternator

Hua Bai

Steven Pekarek
Missouri University of Science and Technology

Jerry L. Tichenor

Walter Eversman
Missouri University of Science and Technology, eversman@mst.edu

et. al. For a complete list of authors, see https://scholarsmine.mst.edu/ele_comeng_facwork/1084

Recommended Citation

H. Bai et al., "Incorporating the Effects of Magnetic Saturation in a Coupled-Circuit Model of a Claw-Pole Alternator," *IEEE Transactions on Energy Conversion*, Institute of Electrical and Electronics Engineers (IEEE), Jan 2007.
The definitive version is available at https://doi.org/10.1109/TEC.2006.875444

Incorporating the Effects of Magnetic Saturation in a Coupled-Circuit Model of a Claw–Pole Alternator

Hua Bai, *Member, IEEE*, Steven D. Pekarek, *Member, IEEE*, Jerry Tichenor, *Member, IEEE*, Walter Eversman, Duane J. Buening, Gregory R. Holbrook, and Ronald J. Krefta

***Abstract*—A method of representing the effects of magnetic saturation in a coupled-circuit model of a claw–pole alternator is presented. In the approach considered, the airgap flux density produced by each winding is expressed as a function of magnetic operating point. A challenge in the implementation is that the airgap flux densities consist of several significant harmonics, each of which changes at a distinct rate as iron saturates. Despite this complication, it is shown that relatively simple measurements can be used to determine model parameters. The model is implemented in the analysis of several alternator/rectifier systems using a commercial state-model-based circuit analysis program. Comparisons with experimental results over a wide range of speeds and operating conditions demonstrate its accuracy in predicting both the steady state and transient behavior of the systems.**

***Index Terms*—Electromagnetic torque, rectifiers, state model, synchronous machines.**

I. Introduction

ADVANCES in power electronic devices are providing the capability to consider new topologies in many finite-inertia power systems, including those of automobiles, aircraft and spacecraft. Design of these systems often focuses on issues of cost, power density, stability, and harmonic performance (including vibration and acoustic noise). Effectively addressing these issues requires the use of accurate models of key components, as well as utilizing efficient methods of developing and solving system-level models.

A primary component used in many finite-inertia power systems is a claw–pole, or "Lundell," machine. To model these machines most analysts have relied on finite element (FE) or magnetic equivalent circuit (MEC) techniques [1]–[7]. These have been shown to provide accurate results and are valuable tools in machine design. However, their use in system-level analysis can be limited by numerical requirements or the complexity in deriving the model. For example, using a coupled FE/circuit approach to model a single machine/rectifier over an electrical cycle requires 8 h of CPU time on a 2×552-MHz processor workstation [4]. To model the machine using a MEC approach requires considerably less time. In [5], it is shown that a 40th-order MEC model of a machine connected to a circuit-based model of a rectifier can be simulated in several minutes. Although relatively efficient numerically, the effort required to derive a 40th-order model is significant.

As an alternative to a full-order MEC model, it has been shown that it is possible to derive low-order models of a claw–pole machine, assuming the permeability of the stator and rotor iron is infinite. In [8], Fourier-series-based expressions of the airgap flux density are used to determine self- and mutual-inductances of the field and stator windings. The resulting inductances form the basis of a sixth-order coupled-circuit model that has been shown to accurately portray the dynamics of the machine in the linear magnetic region.

In this paper, a method of incorporating the effects of magnetic saturation in the coupled-circuit model is presented. In the machine considered, harmonics introduced by stator windings, stator slots, and rotor saliency all have a significant effect on machine and system performance. In order to accurately capture machine behavior, the harmonics that change with iron saturation are first identified. Subsequently, a magnetic operating point is expressed as a function of magnetizing flux linkage. Closed form expressions relating harmonics to the magnetic operating point are then used to establish self- and mutual-inductances of the machine.

Since the model requires characterization of a constructed machine, it cannot replace FE or MEC as a tool for selecting initial geometries. However, due to its relative simplicity and low number of states, it is useful in the analysis of machine performance and the design of systems in which claw–pole machines are applied. To demonstrate its utility, the model is implemented in the simulation of both delta- and wye-connected six-pulse alternator/rectifier systems using a state-model-based circuit analysis program. Comparisons with experimental results over a range of operating conditions demonstrate the accuracy of the model in predicting both the steady-state and transient dynamics of the machine.

II. Background

The machine modeled has three full-pitch wave-wound concentrated stator windings and 12 rotor poles shaped in the form of a claw. The rotor structure of the machine modeled is shown in Fig. 1. A simplified diagram of a single pole of the stator/rotor with the axes and angles that are used for machine analysis is

Manuscript received November 6, 2003; revised January 25, 2005. Paper no. TEC-000328-2003.

H. Bai is with the Linear Technology Corp., Milpitas, CA 95035-7417 USA (e-mail: hbai15@hotmail.com).

S. D. Pekarek is with the Department of Electrical Engineering, Purdue University, West Lafayette, IN 47905 USA (e-mail: spekarek@purdue.edu).

J. L. Tichenor is with the Department of Electrical and Computer Engineering, University of Missouri-Rolla, Rolla, MO 65409 USA (e-mail: jticheno@umr.edu).

W. Eversman is with the Department of Mechanical Engineering, University of Missouri—Rolla, Rolla, MO 65409 USA (e-mail: eversman@umr.edu).

D. Buening and G. Holbrook were with Delphi Corp., Kokomo, IN 46904 USA. They are now with Delco Remy, World Headquarters and U.S. Technical Center, Anderson, IN 46013 USA.

R. Krefta is with Delphi Corp., Kokomo, IN 46904 USA (e-mail: ron.j.krefta@delphi.com).

Digital Object Identifier 10.1109/TEC.2006.875444

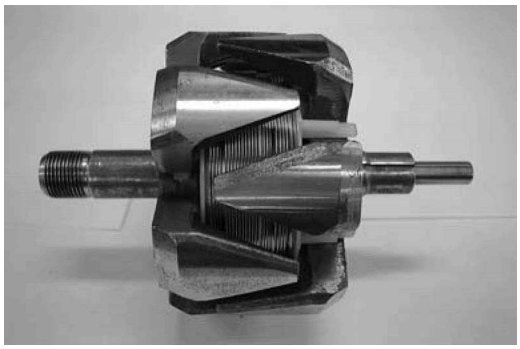

Fig. 1. Rotor structure of claw–pole alternator.

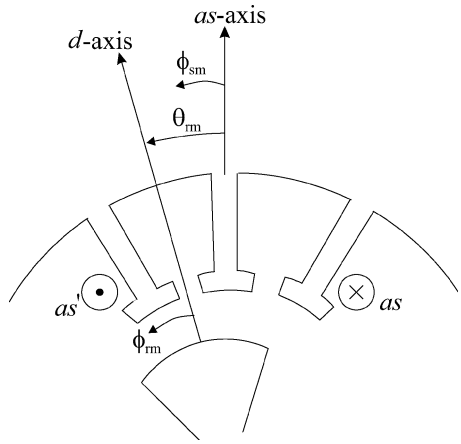

Fig. 2: Illustration of reference axes, angles, and dimensions.

shown in Fig. 2. The angles shown include the mechanical rotor position $\theta_{\rm rm}$, the angular position on the stator relative to the as-axis $\phi_{\rm sm}$, and the angular position on the rotor relative to the d-axis $\phi_{\rm rm}$. Herein corresponding "electrical" angles, $\theta_{\rm r}, \phi_{\rm s}$, and $\phi_{\rm r}$ are defined by multiplying $\theta_{\rm rm}, \phi_{\rm sm}$, and $\phi_{\rm rm}$ by the number of pole pairs.

In the coupled-circuit model, the electrical dynamics of the stator and rotor circuits are represented in the form

$$\begin{bmatrix} \mathbf{v}_{\rm abcs} \\ v_{\rm fd} \end{bmatrix} = \begin{bmatrix} \mathbf{r}_{\rm s} & 0 \\ 0 & r_{\rm fd} \end{bmatrix} \begin{bmatrix} \mathbf{i}_{\rm abcs} \\ i_{\rm fd} \end{bmatrix} + \begin{bmatrix} \lambda_{\rm abcs} \\ \lambda_{\rm fd} \end{bmatrix} \quad (1)$$

$$\begin{bmatrix} \mathbf{v}_{\rm abcs} \\ v_{\rm fd} \end{bmatrix} = \begin{bmatrix} \mathbf{L}_{\rm ss}(\theta_{\rm r}) & \mathbf{L}_{\rm sfd}(\theta_{\rm r}) \\ \mathbf{L}_{\rm fds}(\theta_{\rm r}) & L_{\rm fd}(\theta_{\rm r}) \end{bmatrix} \begin{bmatrix} \mathbf{i}_{\rm abcs} \\ i_{\rm fd} \end{bmatrix} \quad (2)$$

where v, i, and λ represent the voltage, current, and flux linkages of respective windings and $p = d/dt$. The matrices $\mathbf{r}_{\rm s}, \mathbf{L}_{\rm ss}(\theta_{\rm r}), \mathbf{L}_{\rm sfd}(\theta_{\rm r})$, and $\mathbf{L}_{\rm fds}(\theta_{\rm r})$ contain the stator winding resistance and the self- and mutual-inductances between windings, respectively. The scalars $r_{\rm fd}$ and $L_{\rm fd}(\theta_{\rm r})$ represent the resistance and self-inductance of the field winding.

If the machine is operated in the linear magnetic region, it has been shown that the dynamic performance can be modeled with reasonable accuracy, using inductances that are derived from Fourier-series-based expressions for the airgap flux density [8]. Specifically, the field and stator phase-a self-inductances, $L_{\rm fd}(\theta_{\rm r})$ and $L_{\rm asas}(\theta_{\rm r})$, and field to phase-$a$ mutual inductance $L_{\rm fdas}(\theta_{\rm r})$ can be obtained using

$$L_{\rm fd} = L_{\rm lfd} + N_{\rm fd} \int_0^l \int_{\frac{-\pi}{2}}^{\frac{\pi}{2}} B_{\rm fd}(\phi_{\rm r}, \theta_{\rm r}, z)(r d\phi_{\rm r}) dz \quad (3)$$

$$L_{\rm asas} = L_{\rm ls} + N_{\rm s} \int_0^l \int_{\frac{-\pi}{2}}^{\frac{\pi}{2}} B_{\rm air}(\phi_{\rm s}, \theta_{\rm r}, z)(r d\phi_{\rm s}) dz \quad (4)$$

$$L_{\rm fdas} = N_{\rm fd} \int_0^l \int_{\frac{-\pi}{2}}^{\frac{\pi}{2}} B_{\rm air}(\phi_{\rm r}, \theta_{\rm r}, z)(r d\phi_{\rm r}) dz \quad (5)$$

where $B_{\rm fd}$ and $B_{\rm as}$ are the airgap flux densities due to current in the field and phase-a stator windings, respectively; l is the length of the stator core; z is the axial position in the airgap; r is the radius to the midpoint of the airgap; $N_{\rm fd}$ and $N_{\rm as}$ are the turns of the field and phase-a windings; and $L_{\rm lfd}$ and $L_{\rm ls}$ are leakage inductances. Expressions for the remaining inductances are derived using similar expressions.

The flux density in the airgap is modeled starting with magnetic equivalent circuit techniques applied to the airgap. Specifically the airgap flux density is modeled as a scalar quantity representing flux density in a direction normal to the surfaces of the iron. The tangential and axial directions of the flux density are not considered. The representation of the normal component is established by multiplying the MMF created by the respective winding by an airgap permeance function. The MMF is assumed to be a function of circumferential position in the airgap, i.e., at each circumferential position it is assumed uniform in the axial direction. The rotor and stator are both salient structures. The effects of rotor and stator saliency are modeled using distinct functions that represent the increase in reluctance around noniron structures. Specifically, the airgap flux densities used to calculate inductances are represented as

$$B_{\rm fd}(\phi_{\rm r}, \phi_{\rm s}, z) = {\rm MMF}_{\rm fd}(\phi_{\rm r}) \gamma_{\rm r}(\phi_{\rm r}, z) sl(\phi_{\rm s}) \quad (6)$$

$$B_{\rm as}(\phi_{\rm r}, \phi_{\rm s}, z) = {\rm MMF}_{\rm as}(\phi_{\rm as})(\phi_{\rm s}) \gamma_{\rm r}(\phi_{\rm r}, z) sl(\phi_{\rm s}) \quad (7)$$

where $\gamma_{\rm r}$ is the airgap permeance that is used to account for changes in airgap length due to rotor saliency, sl is a function that represents the reduction of the flux density around stator slots, and ${\rm MMF}_{\rm fd}$ and ${\rm MMF}_{\rm as}$ denote the normalized airgap due to current in the field and phase-a winding, respectively. Herein, all values of MMF are normalized to the respective winding current. Using the angles shown in Fig. 2, ${\rm MMF}_{\rm as}$ and ${\rm MMF}_{\rm fd}$ are represented in series form as

$${\rm MMF}_{\rm as} = \sum_{k=1}^{\infty} F_{\rm ask} \cos(k\phi_{\rm s}) \quad (8)$$

$${\rm MMF}_{\rm fd} = \sum_{k=1}^{\infty} F_{\rm fdk} \cos(k\phi_{\rm r}) \quad (9)$$

where $F_{\rm ask}$ and $F_{\rm fdk}$ are expressed as a function of coil turns. To evaluate $\gamma_{\rm r}$, it is assumed that the airgap length between claws is sufficiently large that the airgap permeance is zero. Using this assumption, the permeance has two possible values

$$\gamma_{\rm r}(\phi_{\rm r}, z) = \begin{bmatrix} \frac{\mu_0}{g} \\ 0 \end{bmatrix} \begin{matrix} \text{above a rotor claw} \\ \text{between rotor claws} \end{matrix} \quad (10)$$

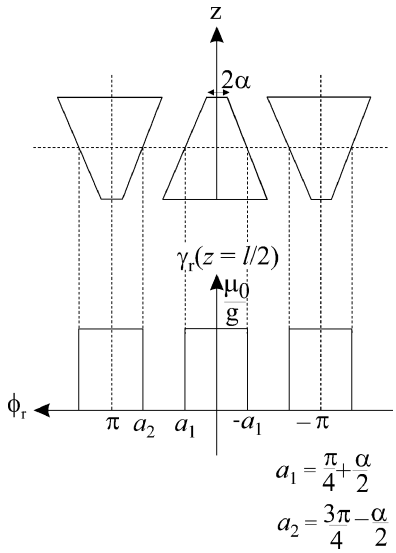

Fig. 3. Airgap permeance as a function of $\phi_{\rm r}$ at $z = l/2$.

where μ_0 is the permeability of air and g is the length of the airgap. The reliance on both the angular position $\phi_{\rm r}$, and axial position z, results from the claw structure. To establish a closed-form expression that represents (10), a one-dimensional (1-D) series evaluation is considered first. In particular, at any given axial position z, it is possible to establish a Fourier-series representation of $\gamma_{\rm r}$ as a function of $\phi_{\rm r}$. To illustrate, the permeance versus the angular position on the rotor $\phi_{\rm r}$, at the midpoint of the claw length $(z = l/2)$ is shown in Fig. 3. The angles a_1 and a_2 defined in Fig. 3 form the intervals of integration in the evaluation of the Fourier coefficients. Using these angles a series expression for the permeance at $(z = l/2)$ can be written as

$$\gamma_{\rm r}\left(\phi_{\rm r}, \frac{l}{2}\right) = \sum_{k=0}^{\infty} \gamma_{ak}\left(\frac{l}{2}\right)\cos(k\phi_{\rm r}) \tag{11}$$

where

$$\gamma_{ak}\left(\frac{l}{2}\right) = \frac{2}{\pi}\frac{\mu_0}{g}\left\{\int_0^{a_1}\cos(k\phi_{\rm r})d\phi_{\rm r} + \int_{a_2}^{\pi}\cos(k\phi_{\rm r})d\phi_{\rm r}\right\}. \tag{12}$$

In general, a 1-D series expansion for permeance can be defined at any axial position by rederiving expressions for the angles a_1 and a_2. If the rotor is symmetric, and $\phi_{\rm r}$ is defined from the d-axis, the angles are given by [8]

$$a_1(z) = \frac{\pi}{2} - \frac{z\pi}{2l} + \frac{z\alpha}{l} \tag{13}$$

$$a_2(z) = \pi - \alpha - \frac{z\pi}{2l} + \frac{z\alpha}{l} \tag{14}$$

Using (13) and (14) to evaluate the Fourier coefficients at each position along the axis, a 2-D permeance can be expressed in a general form

$$\gamma_{\rm r}(\phi_{\rm r}, z) = \sum_{k=0}^{\infty}\gamma_{ak}(z)\cos(k\phi_{\rm r}) + \sum_{k=1}^{\infty}\gamma_{bk}(z)\sin(k\phi_{\rm r}) \tag{15}$$

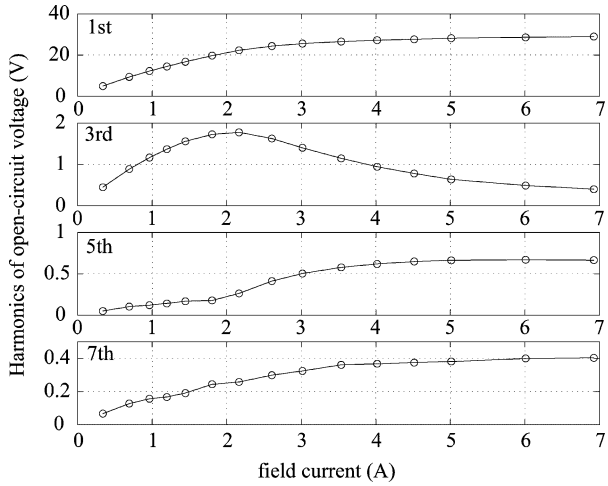

Fig. 4. Harmonics of open-circuit phase-a flux linkage.

where, for a symmetrical claw [8]

$$\gamma_{a0} = \frac{\mu_0}{g\pi}(\pi + 2\alpha) \tag{16}$$

$$\gamma_{ak}(z) = \frac{2\mu_0}{k\pi g}\left[\sin\left(\frac{k}{2}\left(\pi - \frac{z\pi}{l} + \frac{2z\alpha}{l}\right)\right)\right] + \sin\left[\frac{k}{2}\left(-2\pi + \frac{z\pi}{l} + 2\alpha - \frac{2z\alpha}{l}\right)\right], \quad k \geq 1 \tag{17}$$

$$\gamma_{bk}(z) = 0. \tag{18}$$

The slot function, sl, is defined as having a value of 1 at the positions of $\phi_{\rm s}$ where a tooth is present and a value of x where a slot is located. The value of x represents the ratio of the flux density at the center of the slot to the flux density at the center of the stator tooth assuming a uniform rotor structure. Its value is obtained from the graphical analysis of flux pulsation around slots [9]. In general, a series representation of the form

$$sl = sl_0 + \sum_{m=1}^{\infty} sl_{6m}\cos(6m\phi_{\rm s}) \tag{19}$$

can be used to fit the slot function. It is noted that when using this technique sl_0 is equal to the inverse of the Carter coefficient [10].

III. Establishing the Effects of Magnetic Saturation

Multiplication of the series in (8)–(9), (15), and (19) results in the expressions for airgap flux density [(6) and (7)] that is used to establish the inductances of the coupled-circuit model. To evaluate the behavior of the machine in the nonlinear magnetic region using the coupled-circuit model, the influence of saturation on each of the harmonics must be considered. To illustrate this point, it is useful to observe the magnitude of the measured open-circuit stator phase-a voltage harmonics as a function of field current, which is shown in Fig. 4. The open-circuit voltages were measured using a digital oscilloscope with the machine running at 1800 r/min. The harmonic components were

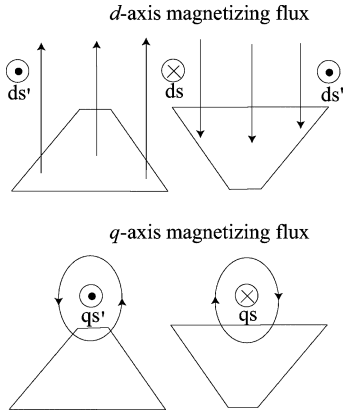

Fig. 5. d- and q-axis magnetizing paths.

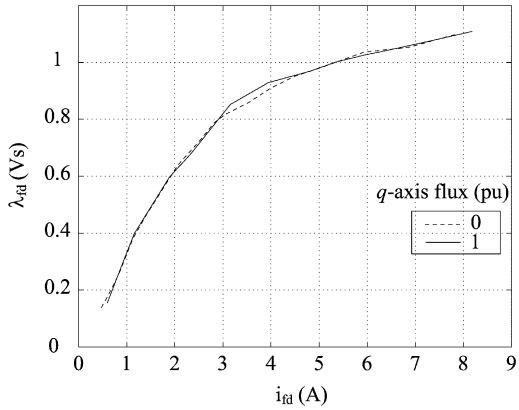

Fig. 6. Field flux linkage versus field current at different levels of q-axis flux.

determined using a Fourier analysis. Results presented herein utilize data from a single phase to establish all self- and mutual-inductances. If an imbalance between windings is desired to be modeled, open-circuit voltages of each phase winding are required to complete the modeling approach described, herein. From Fig. 4, it can be seen that the magnetizing curves of each of the harmonics are quite different. It is interesting to note that the third harmonic decreases significantly in saturation. Additionally, there is an abrupt change in the fifth harmonic where it sharply increases before leveling in heavy saturation. These behaviors indicate that the magnetic flux distribution across a claw changes with the operating conditions of the machine.

To model saturated behavior, a nonlinear relationship is established between harmonic components of airgap flux density and magnetizing flux linkage. Prior to deriving the approach in detail, it is useful to define the magnetizing paths used as a basis for the model and describe a measurement used to justify the definition of a magnetic operating point. In Fig. 5, the paths of the direct (d)- and quadrature (q)-axis magnetizing flux are shown. The d-axis has been defined in the direction of field-winding flux linkage (IEEE standard for wound-rotor synchronous machines). The q-axis is defined orthogonal to the d-axis. For the given machine, this is in a direction tangential to the surface of the claw at its peak point. Although at first glance of Fig. 5, this appears to be a break from convention, it is consistent with the definition of q-axis for salient pole synchronous machines used in bulk-utility applications.

In the machine modeled, the ampere turns of the field winding are sufficient to saturate the d-axis under typical values of field current. Neglecting eddy currents, only stator current produces flux in the q-axis. As an approximation, it was assumed that the magnetic operating point is determined primarily by the direct axis magnetizing flux. To justify this approximation, the influence of q-axis flux on d-axis saturation levels was established through a series of measurements. Therein, the d-axis of the rotor was placed directly beneath the phase-a stator winding. The phase b- and c-windings were open circuited and the phase-a winding was energized with a dc current to produce q-axis flux. Holding the phase-a current fixed, step changes in voltage were applied to the field winding and the field flux (d-axis) was measured with respect to field current to generate a d-axis saturation curve. The phase-a current was then increased to yield rated (1 pu) q-axis flux linkage and the study was repeated. The results of the experiment are shown in Fig. 6. Nearly identical curves were obtained for all q-axis flux levels between 0 and 1 pu.

IV. Incorporating the Effect of Saturation in the Coupled-Circuit Model

Using the d-axis magnetizing flux as the magnetic operating point, it is theoretically possible to measure inductance at different levels of d-axis flux to generate a look-up-table or closed-form expression for each winding's self- and mutual-inductances. One of the practical difficulties in pursuing such an approach is that measuring mutual inductance between stator windings while maintaining a constant d-axis flux is very difficult. A second complication is that each inductance must be characterized over an entire cycle of rotor angular position, which requires significant effort. To simplify the modeling procedure, the effect of saturation on airgap flux density, rather than inductance, is considered. From (6) and (7), it is clear that the airgap flux density produced by each winding is a function of $\gamma_{\rm r}$, MMF, and sl. $\gamma_{\rm r}$ is independent of iron saturation. Harmonics of airgap MMF change significantly in saturation and their values cannot be determined analytically. However, it is known, using the relationship $L_{\rm asfd} = L_{\rm fdas}$, that $\rm MMF_{fd}$ harmonics are related to $\rm MMF_{as}$ harmonics by the stator/field turns ratio. The slot function, sl, is based upon the evaluation of flux behavior around stator slots assuming that the relative permeability of the stator teeth is much larger than unity. As the relative permeability of the stator teeth decreases, the coefficients of the slot function may change. For simplicity in deriving the saturated model, changes in the slot function were initially neglected. Results (described in Section VII) obtained using this approximation have been reasonably accurate. If saturation of the slot function is considered, the measurement procedure required to obtain model parameters is significantly more complex.

Assuming changes in the teeth/slot flux ratio can be neglected, knowledge of the harmonics of a stator open circuit voltage (along with values of leakage inductance) are sufficient to determine all winding self- and mutual-inductances. Specifically, by

differentiating (5) [using (7) as the flux density], and the relationship that $L_{\rm asfd} = L_{\rm fdas}$, one can express the back-electromotive force (emf) harmonics in the form

$$\boldsymbol{v}_{\rm asoc} = \mathbf{A}(sl, \gamma)\mathbf{F} \tag{20}$$

where $\boldsymbol{v}_{\rm asoc}$ is a vector that contains the amplitudes of open-circuit voltage harmonics and $\boldsymbol{F}$ is a vector containing the amplitude of harmonics of airgap MMF. In general, one can use an increasing number of back-emf harmonics to determine an increasing number of MMF harmonics. In the machine considered, $F_1 \ldots, F_7$ were determined using $v_{\rm asoc1}, \ldots, v_{\rm asoc7}$. Although the evaluation of (5) to obtain (20) appears complicated, symbolic solution of the integral in (5) is relatively straightforward using commercial software packages such as Mathcad or Maple.

From the back-emf harmonic amplitudes, the MMF harmonics are determined as a function of d-axis current. To define a d-axis current in terms of model parameters, the field winding flux linkage is expanded in terms of stator and rotor currents as

$$\begin{aligned}\lambda_{\rm fd} &= L_{\rm lfd} i_{\rm fd} + L_{\rm fd} i_{\rm fd} + L_{\rm asfd} i_{\rm as} \\ &\quad + L_{\rm bsfd} i_{\rm bs} + L_{\rm csfd} i_{\rm cs}.\end{aligned} \tag{21}$$

The first term on the right-hand side of the equal sign in (21) represents the leakage flux. The remaining terms on the right form the d-axis magnetizing flux. For convenience, magnetizing flux is expressed in the form

$$\lambda_{\rm md} = L_{\rm fd}\left(i_{\rm fd} + \frac{L_{\rm asfd}}{L_{\rm fd}} i_{\rm as} + \frac{L_{\rm asfd}}{L_{\rm fd}} i_{\rm bs} + \frac{L_{\rm csfd}}{L_{\rm fd}} i_{\rm cs}\right). \tag{22}$$

The d-axis magnetizing current is defined as

$$i_{\rm md} \triangleq i_{\rm fd} + \frac{L_{\rm asfd}}{L_{\rm fd}} i_{\rm as} + \frac{L_{\rm bsfd}}{L_{\rm fd}} i_{\rm bs} + \frac{L_{\rm csfd}}{L_{\rm fd}} i_{\rm cs}. \tag{23}$$

V. Saturation of Leakage Paths

Since a significant portion of the rotor leakage flux path is through air, saturation of the rotor leakage inductance was neglected. However, saturation of the stator leakage inductance is considered within the model. To evaluate the effects of saturation, the stator leakage inductance was first partitioned into the end-turn and slot components. Specifically

$$L_{\rm ls} = L_{\rm lend} + L_{\rm lslot} \tag{24}$$

where $L_{\rm lend}$ is the end-turn leakage and $L_{\rm lslot}$ is the slot component. It is important to note that $L_{\rm ls}$ does not include what some analysts refer to as leakage due to winding harmonics. The effects of winding harmonics are included within the integral expression for the stator self-inductance. Their behavior in saturation is approximated through modeling changes in the MMF described in Section IV. The end-turn leakage was determined to be 0.1 mH, using expressions derived in [11] and was assumed independent of magnetic operating point. Using the B–H curve of the stator iron, the slot leakage was computed using a simple MEC model of the stator teeth. For the machine considered, with tooth flux densities $B_T = 0$–0.75 T, the slot-leakage is nearly constant at a value of 0.075 mH. At flux densities of $B_T = 1.75$–2 T, the slot-leakage inductance was approximated to be constant at 0.05 mH. Between the value of $B_T = 0.75$–1.75 T, it was assumed that the slot leakage varies linearly between the values of 0.075 and 0.05 mH. Within the model, the tooth flux density is approximated by dividing the d-axis magnetizing flux/pole by the number of teeth/pole and the cross sectional area of a tooth.

VI. Calculation of Electromagnetic Torque

Using an energy balance approach, the electromagnetic torque of an electric machine can be expressed as [12]

$$T_{\rm e} = \frac{P}{2} \times \frac{\partial W_{\rm c}(\mathbf{i}, \theta_{\rm r})}{\partial \theta_{\rm r}} \tag{25}$$

where $W_{\rm c}$ is defined as the coenergy of the coupling field and $\mathbf{i}$ is a vector containing the winding currents. The coenergy can be expressed in terms of the winding flux linkages, currents, and field energy, $W_{\rm f}$, as

$$W_{\rm c}(\mathbf{i}, \theta_{\rm r}) = \sum_j \lambda_j(\mathbf{i}, \theta_{\rm r}) i_j - W_{\rm f}(\mathbf{i}, \theta_{\rm r}) \tag{26}$$

where

$$W_{\rm f}(i, \theta_{\rm r}) = \sum_j \int i_j d\lambda_j. \tag{27}$$

In the machine considered, $j = {\rm as, bs, cs, fd}$. If the machine is operated in the linear magnetic region, it can be shown that [12]

$$\begin{aligned}W_{\rm c}(\boldsymbol{i}, \theta_{\rm r}) = \frac{1}{2}&\begin{bmatrix}\mathbf{i}_{\rm abcs} & i_{\rm fd}\end{bmatrix} \\ &\times \begin{bmatrix}\mathbf{L}_{\rm ss}(\theta_{\rm r}) & \mathbf{L}_{\rm sfd}(\theta_{\rm r}) \\ \mathbf{L}_{\rm fds}(\theta_{\rm r}) & \mathbf{L}_{\rm fdfd}(\theta_{\rm r})\end{bmatrix}\begin{bmatrix}\mathbf{i}_{\rm abcs} \\ i_{\rm fd}\end{bmatrix}.\end{aligned} \tag{28}$$

It is tempting to consider (28) for the evaluation of the coenergy in the nonlinear magnetic region. In particular, the winding flux linkages are related to currents through compensated self- and mutual-inductances. However, the compensation of inductance is a function of state; thus, evaluation of (26) and (27) in the saturated region will not yield (28). Although (28) is not an exact expression for coenergy, evaluation of (25) using (28) (with saturated inductances) represents an approximate expression for torque. The accuracy of the approximation in the claw–pole machine is considered through comparison with experimental results in Section VII.

It is noted that an equation often considered as an expression for the torque of a saturated synchronous machine is [12]

$$T_{\rm e} = \frac{3}{2} \times \frac{P}{2}\left(\lambda^{\rm r}_{\rm ds} i^{\rm r}_{\rm qs} - \lambda^{\rm r}_{\rm qs} i^{\rm r}_{\rm ds}\right) \tag{29}$$

where $\lambda^{\rm r}_{\rm ds}$, $\lambda^{\rm r}_{\rm qs}$, $i^{\rm r}_{\rm qs}$, and $i^{\rm r}_{\rm ds}$ are the stator flux linkages and currents expressed in the rotor reference frame through Park's transformation. Although convenient, (29) can only be shown to be exact if the relationship between the flux linkages and currents is independent of rotor position. This can be shown through straightforward extension of the analysis of torque described in [13]. Transformation of the coupled-circuit model of the machine considered does not eliminate rotor-position-dependent

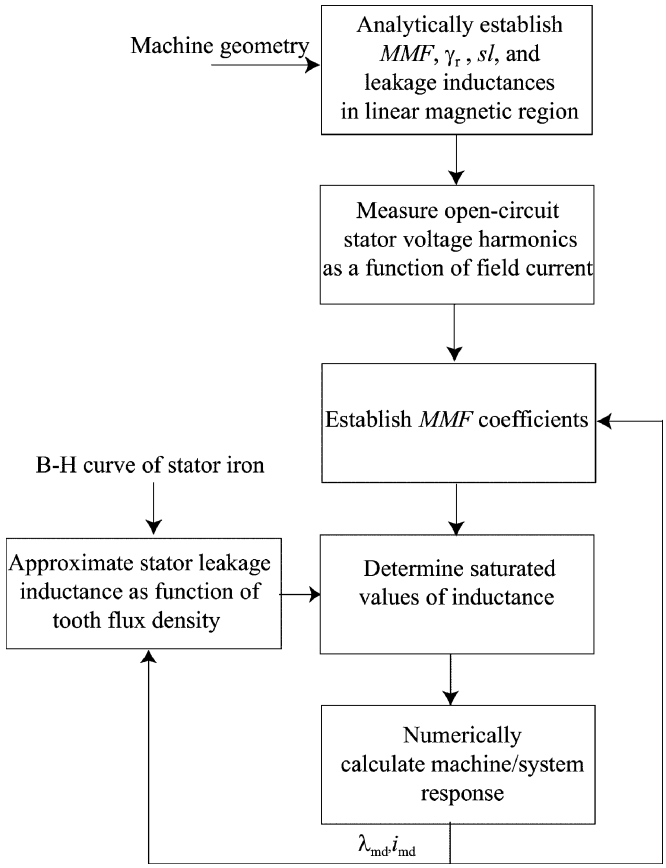

Fig. 7. Steps applied to model machine in saturation.

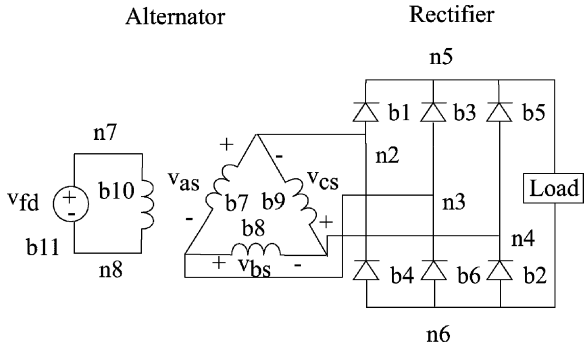

Fig. 8. Alternator/rectifier system.

TABLE I
MACHINE PARAMETERS

Stator outside diameter = 0.13 m	Stator length = 0.027 m	$N_{fd} = 300$
$N_{as} = 11$	$P = 12$	$r_s = 0.11\ \Omega$
$r_{fd} = 2.4\ \Omega$	$L_{lfd} = 53$ mH	

inductances; thus, (29) can only be regarded as an approximate expression for torque produced in either the saturated or unsaturated regions. The accuracy of the approximation is considered through comparison with experimental results in Section VII.

An exact closed-form expression for torque is difficult to obtain analytically. As an alternative, to provide an "exact" expression within the model, the coenergy is calculated numerically from (26) and the torque obtained through numerical differentiation (with respect to rotor position) of (25).

VII. Model Implementation and Validation

A diagram that illustrates the necessary steps to create the model of the machine in saturation is shown in Fig. 7. In many applications, the claw–pole alternator is connected to a six-pulse rectifier as shown in Fig. 8. To validate the saturated lumped-parameter model, three machine/rectifier studies were implemented using the commercial simulation language ACSL [14]. Several parameters of the machine studied are provided in Table I.

The state model of the machine/rectifier was established, using the automated state model generation algorithm (ASMG) derived in [15]. In the application of the ASMG, a system is described by pertinent branch parameters and circuit topology, similar to the syntax used in commercial circuit analysis programs, including Saber [16] and Spice [17]. The composite-system state equations are established algorithmically and are solved using standard numerical integration algorithms. Within the ASMG, winding flux linkages were chosen as state variables. Upon completion of an integration cycle, the stator currents are determined using (2). The d-axis magnetizing current is determined using (23), after which the harmonics and stator leakage inductance are updated. Winding inductances are calculated using the updated values of MMF.

It is noted that the solutions to the integrals used to calculate inductance are represented as a series within the model. The series expansions are obtained using a commercial symbolic mathematical evaluation program.

In the first study, the steady state operations of both delta- and wye-connected machine/rectifier systems were investigated. For both cases, the rotor speed was held constant at 1900 r/min and the load resistance was set to 0.344 Ω. The field voltage was set to produce a 5-A field current in steady state. At the respective conditions, the d-axis magnetizing current was on the order of 4 A. From Fig. 3, it can be seen that for a 4-A magnetizing current the machine operates in the nonlinear magnetic region. The measured and simulated phase current, phase voltage, and dc output current of the delta-connected machine are shown in Fig. 9. Measured and simulated results for the wye-connected machine are shown in Fig. 10. As shown, the measured and simulated responses of both wye- and delta-connected machines are in strong agreement. There is a greater difference between simulated and measured current in the delta-connected machine that is attributed to a slight difference between simulated and measured third harmonic current that circulates in the stator windings. The machine studied has a slight imbalance between phase windings due to manufacturing, which has not been included in the machine model. In calculating the response, a fourth-order Runge–Kutta–Fehlberg algorithm was used with a maximum and minimum time step of 10^{-3} and 10^{-7} s, respectively. The simulation required approximately 0.03 s of CPU time to obtain the dynamic response using a 1-GHz Pentium PC.

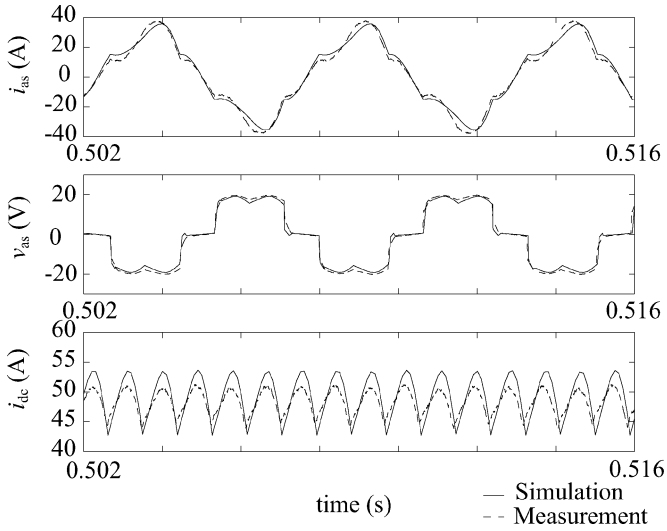

Fig. 9. Results of simulation and measurement for delta-connected machine.

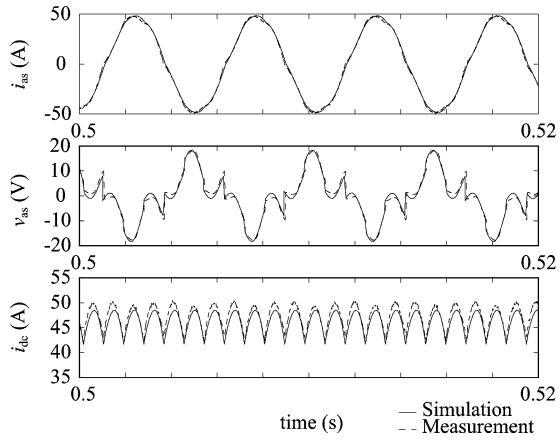

Fig. 10. Results of simulation and measurement for wye-connected machine.

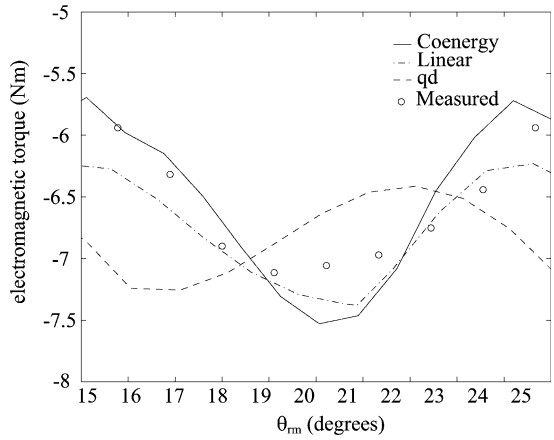

Fig. 11. Simulated and measured electromagnetic torque for wye-connected machine.

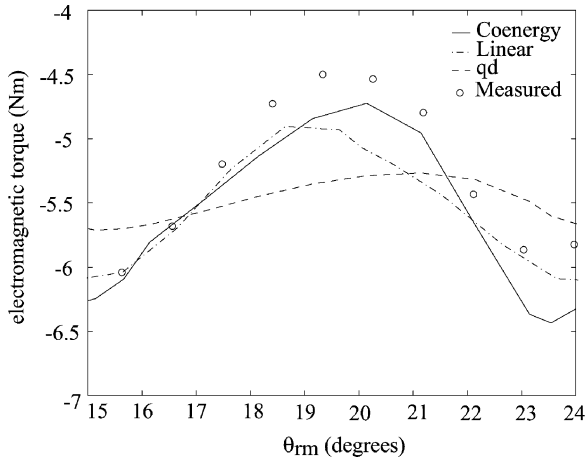

Fig. 12. Simulated and measured electromagnetic torque for delta-connected machine.

For both wye- and delta-connected machines, the three techniques that are described in Section VI were used to determine the electromagnetic torque. Specifically, in the first method, torque is calculated through numerical evaluation of (20) and (21). In the second method, the coenergy is approximated using (23) with saturated inductances. The resulting expression is used to determine a closed-form expression for torque using (20). In the third method, the expression given in (24) is applied. The results of the three methods are shown with measured data in Figs. 11 and 12. To measure electromagnetic torque, the rotor speed was fixed with the respective load connected to the dc terminals. The stator and field currents were then measured with respect to rotor position.

Once the measured values of current versus rotor position were obtained, the machine was stopped and the rectifier disconnected from the terminals. Individual power supplies were then placed across each of the stator windings and the field winding. The rotor was then locked at an arbitrary angle. Using the individual power supplies, the stator and field currents were adjusted to the values that were measured at the respective angle when the machine was running with the rectifier connected. The torque was then measured using an in-line torque transducer. The measurement was repeated at approximately one degree (mechanical) increments. From Figs. 9 and 10, it can be seen that the torque is not constant in steady state. This is due to harmonics in the airgap flux density that result from stator current, stator slots, and rotor saliency. Comparing measured and simulated responses, it is seen that the average torque is reasonably predicted by all three methods. The torque at each respective rotor angle is predicted with modest success using both the numerical evaluation of coenergy and the expression for coenergy derived in the linear region with saturated inductance values. It is interesting to note that when using (21), one obtains a much less accurate value of the torque at each angular position.

In the second study, a transient condition was simulated. Therein, it was assumed that the delta-connected machine was initially operating in the steady state at 1800 r/min with a base load resistance of 1.0-Ω connected to the dc output terminals. The field voltage was adjusted to produce 5-A field current in the steady-state. The load was then switched to a value of 0.2-Ω. The measured and simulated results of field current and dc current are depicted in Fig. 13. As shown, the measured and simulated transient responses are in very good agreement.

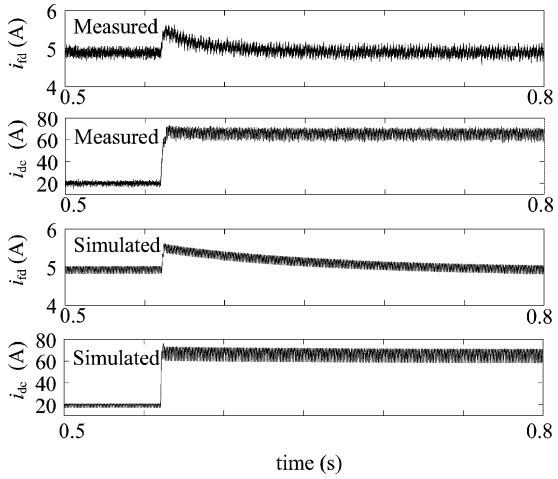

Fig. 13. Transient response of delta-connected machine.

TABLE II
MEASURED AND SIMULATED MACHINE/RECTIFIER OUTPUT CURRENT

Speed (RPM)	Measured (A)	Simulated (A)
1600	50.8	50.3
3000	92.2	95.3
6000	104.3	108.5

In the final study, the performance of the delta-connected machine/rectifier with a 14-V battery load was simulated at rotor speeds of 1600, 3000, and 6000 r/min. The field current was held constant at 5 A. The average output current was calculated at each speed and compared with measured values. As speed increases the d-axis magnetizing current decreases from over 4 A to approximately 2 A, which provides a wide range of magnetic operating points to evaluate the model. The results are shown in Table II. Comparing values, it can be seen that the error is less than 5% at all given speeds.

It is noted that the rotor pole faces and core are constructed of nonlaminated iron. Therefore, the effects of eddy-currents can become a design issue as rotor speed increases. In [18]–[20], a finite element approach has been used to predict the loss attributed to eddy currents in the rotor of a claw–pole machine. Extracting from the data presented at 1800 r/min (180-Hz electrical), eddy current losses are practically insignificant. At 6000 r/min (600-Hz electrical), the loss attributed to rotor eddy currents is roughly 10% of the input power. However, at 10 000 r/min (1000-Hz electrical), the loss is roughly 20% of the input power. In addition, as speeds approach 10 000 r/min, loss due to eddy currents in the stator laminations becomes appreciable.

Based upon our experience and the results presented in [18]–[20], it is concluded that the model that has been developed is a useful tool for modeling machines at speed ranges that are of typical commercial interest (below 6000 r/min). Above this level, higher order models are likely required to accurately predict machine behavior. Modeling the effects of eddy currents adds significant complexity to the saturated coupled-circuit model. This remains a topic of ongoing investigation.

VIII. CONCLUSION

The incorporation of saturation within a coupled-circuit model of a claw–pole alternator is described. An important finding is that for the machine considered, the direct axis magnetizing flux can be used to define a magnetic operating point. Model parameters can be determined through evaluation of open circuit stator voltage. The models have been implemented in the simulation and analysis of several alternator/rectifier systems using a state-model-based circuit analysis program. Comparisons with experimental results demonstrate a reasonable accuracy in predicting the steady-state and transient performance of the machine.

REFERENCES

[1] I. Ramesohl, G. Henneberger, S. Kuppers, and W. Hadrys, "Three dimensional calculation of magnetic forces and displacements of a Claw-pole generator," *IEEE Trans. Magn.*, vol. 32, no. 3, pp. 1685–1688, May 1996.
[2] R. Wang and N. A. O. Demerdash, "Extra high speed modified Lundell alternator parameters and open/short circuit characteristics from global 3D-FE magnetic field solutions," *IEEE Trans. Energy Convers.*, vol. 7, no. 2, pp. 330–341, 1992.
[3] B. H. Chen, J. D. Cote, and M. L. Hull, "Claw-pole generator simulation with Ansys/Saber for performance and noise improvement," presented at the Ansys Inc. Conf., 1997.
[4] H. Bai, "Alternator finite element simulation," Technical presentation at Delphi Automotive Systems, Aug. 17, 2000.
[5] V. Ostovic, J. M. Miller, V. Garg, R. D. Schultz, and S. Swales, "A magnetic equivalent circuit based performance computation of a Lundell alternator," *IEEE Trans. Ind. Appl.*, vol. 35, no. 4, pp. 825–830, Jul.–Aug. 1999.
[6] M. Hecquet and P. Brochet, "Modeling of a Claw-pole alternator using permeance network coupled with electric circuits," *IEEE Trans. Magn.*, vol. 31, no. 3, pp. 2131–2134, May 1995.
[7] S. Kuppers and G. Henneberger, "Numerical procedures for the calculation and design of automotive alternators," *IEEE Trans. Magn.*, vol. 33, no. 2, pp. 2022–2025, Mar. 1997.
[8] H. Bai, S. Pekarek, and J. Tichenor *et al.*, "Derivation of a coupled-circuit model of a Claw-Pole machine with concentrated stator windings," *IEEE Trans. Energy Convers.*, vol. 17, no. 1, pp. 32–38, Mar. 2002.
[9] R. L. Wiseman, "Graphical determination of magnetic fields with practical applications to salient-Pole machine design," *Trans. AIEE*, pp. 430–437, May 1927.
[10] M. G. Say, *Alternating Current Machines*. New York: Wiley, 1976.
[11] J. Engstrom, "Inductances of slotless machines," in *Proc. IEEE Nordic Workshop Power and Industrial Electronics*, Aalborg, Denmark, Jun.2000, pp. 266–270.
[12] P. C. Krause, O. Wasynczuk, and S. D. Sudhoff, *Analysis of Electric Machinery*. Piscataway, NJ: IEEE Press, 1995.
[13] P. W. Sauer, "Constraints on saturation modeling in AC machines," *IEEE Trans. Energy Convers.*, vol. 7, no. 1, pp. 161–167, Mar. 1992.
[14] E. E. L. Mitchell and J. S. Gauthier, *Advanced Continuous Simulation Language Reference Manual*. Concord, MA: Mitchell and Gauthier Assoc., 1993.
[15] O. Wasynczuk and S. D. Sudhoff, "Automated state model generation algorithm for power circuits and systems," *IEEE Trans. Power Syst.*, vol. 11, no. 4, pp. 1951–1956, Nov. 1996.
[16] L. O. Chua and P. M. Lin, *Introduction to the Saber Simulator*. Beaverton, Oregon: Analogy, Inc., 1991.
[17] L. W. Nagel and D. O. Pederson, "Simulation program with integrated circuit emphasis," University of California Electronic Research LaboratoryMemorandum EAL-M382, Apr. 1973.
[18] C. Kaehler and G. Henneberger, "Transient 3-D FEM computation of eddy-current losses in the rotor of a Claw-Pole alternator," *IEEE Trans. Magn.*, vol. 40, no. 2, pp. 1362–1365, Mar. 2004.
[19] C. Kaehler and G. Henneberger, "Eddy-current computation on a one Pole-Pitch model of a synchronous Claw-Pole alternator," *COMPLEL*, vol. 22, no. 4, pp. 834–846, 2003.
[20] C. Kaehler and G. Henneberger, "Eddy current computation in the claws of a synchronous Claw Pole alternator in generator mode," *IEEE Trans. Magn.*, vol. 38, pp. 1201–1204, Mar. 2002.

Hua Bai (M) was born in Si Mao, Yunnan, China in 1972. He received the B.S.E.E. degree from Tsinghua University, Beijing, China, and the M.S.E.E. degree from China Academy of Railway Sciences, Beijing, in 1995 and 1998, respectively. He received the Ph.D. degree in electrical engineering from the University of Missouri-Rolla, Rolla, MO, in 2001.

Currently, he is working as an Applications Engineer with Linear Technology Corp., Milpitas, CA, where he designs and troubleshoots linear and switching mode power converters. His research interests include the analysis, simulation, and design of electric machines and power converters.

Steven D. Pekarek (S'89–M'96) was born in Oak Park, IL, on December 22, 1968. He received the Ph.D. degree in electrical engineering from Purdue University, West Lafayette, IN, in 1996.

From 1997 to 2004, he was an Assistant (Associate) Professor of Electrical and Computer Engineering at the University of Missouri-Rolla, Rolla, MO. He is currently working as an Associate Professor of Electrical and Computer Engineering at Purdue University and is the Codirector of the Energy Systems Analysis Consortium.

Dr. Pekarek is an Active Member of the IEEE Power Engineering Society, the Society of Automotive Engineers, the Small Motor and Motion Association, and the IEEE Power Electronics Society.

Jerry Tichenor (S'96–M'96) received the B.S. degree (*summa cum laude*) and the M.S. degree from the University of Missouri-Rolla, Rolla, MO, in 1994 and 1996, respectively, both in electrical engineering.

Currently, he is a Research Engineer at the University of Missouri-Rolla. His research interests include power electronics and motor drives.

Walter Eversman received the B.S. degree from Purdue University, West Lafayette, IN and the Ph.D. degree from Stanford University, Stanford, CA, in 1959 and 1964, respectively.

He is Curators Professor of Mechanical and Aerospace Engineering at the University of Missouri-Rolla, Rolla, MO. His research interests include aeroacoustics and structural dynamics.

Dr. Eversman is a registered Professional Engineer in Missouri.

Duane J. Buening was born in Greensburg, IN, on January 26, 1964. He received the B.S. degree in mechanical engineering from Rose Hulman Institute of Technology, Terre Haute, IN, in 1986.

He is currently working with the Forward Development Engineering Group at Delco Remy International, Anderson, where he has been engaged on noise and vibration of rotating electrical machines.

Gregory R. Holbrook was born in Hamilton, OH, on July 9, 1959. He received the B.S. degree in mechanical engineering from the University of Cincinnati, Cincinnati, OH, in 1982.

He is currently working in the Forward Development Engineering group at Delco Remy International, Anderson, IN. His research interests include analytical structural analysis and experimental noise and vibration testing.

Ronald J. Krefta was born in Buffalo, NY. He received the B.S. and M.S. degrees in electrical engineering from Purdue University, West Lafayette, IN, in 1984 and 1985, respectively.

Currently, he is working as a Design Engineer, at Delphi, Kokomo, IN, concentrating on the design of electric machines for vehicle charging systems and hybrid vehicle applications.